Acta Crystallographica Section D
Biological Crystallography
ISSN 1399-0047

Structural insights into the molecular mechanism of *Escherichia coli* SdiA, a quorum-sensing receptor

Truc Kim,[a]‡ Thao Duong,[a]‡ Chun-ai Wu,[a]‡ Jongkeun Choi,[b] Nguyen Lan,[a] Sung Wook Kang,[a] Neratur K. Lokanath,[c] DongWoo Shin,[a] Hye-Yeon Hwang[a]* and Kyeong Kyu Kim[a]*

[a]Department of Molecular Cell Biology, Samsung Biomedical Research Institute, Sungkyunkwan University School of Medicine, Suwon 440-746, Republic of Korea, [b]Department of Cosmetic Science, Chungwoon University, San 29, Namjang, Hongsung, Chungnam 350-701, Republic of Korea, and [c]Department of Studies in Physics, University of Mysore, Manasagangotri, Mysore 570 006, India

‡ These authors contributed equally to this work.

Correspondence e-mail: hyhwang3@gmail.com, kyeongkyu@skku.edu

Received 13 October 2013
Accepted 27 November 2013

PDB references: SdiA, space group C2, 4lfu; space group $P6_522$, 4lgw

Escherichia coli SdiA is a quorum-sensing (QS) receptor that responds to autoinducers produced by other bacterial species to control cell division and virulence. Crystal structures reveal that *E. coli* SdiA, which is composed of an N-terminal ligand-binding domain and a C-terminal DNA-binding domain (DBD), forms a symmetrical dimer. Although each domain shows structural similarity to other QS receptors, SdiA differs from them in the relative orientation of the two domains, suggesting that its ligand-binding and DNA-binding functions are independent. Consistently, in DNA gel-shift assays the binding affinity of SdiA for the *ftsQ*P2 promoter appeared to be insensitive to the presence of autoinducers. These results suggest that autoinducers increase the functionality of SdiA by enhancing the protein stability rather than by directly affecting the DNA-binding affinity. Structural analyses of the ligand-binding pocket showed that SdiA cannot accommodate ligands with long acyl chains, which was corroborated by isothermal titration calorimetry and thermal stability analyses. The formation of an intersubunit disulfide bond that might be relevant to modulation of the DNA-binding activity was predicted from the proximal position of two Cys residues in the DBDs of dimeric SdiA. It was confirmed that the binding affinity of SdiA for the *uvrY* promoter was reduced under oxidizing conditions, which suggested the possibility of regulation of SdiA by multiple independent signals such as quorum-sensing inducers and the oxidation state of the cell.

1. Introduction

Quorum sensing (QS) is a phenomenon that enables bacteria to conduct intraspecies or interspecies cell-to-cell communication *via* accumulated low-molecular-weight signalling molecules or peptides, which are referred to as autoinducers. When the concentration of autoinducer is above a certain threshold, the QS signal can be translated into gene regulation. Consequently, the activities of particular sets of genes involved in diverse biological functions are regulated for appropriate responses, thereby helping the bacteria to recognize and adapt to changes in the surrounding environment. In a typical QS system of Gram-negative bacteria, two key components, an acyl-homoserine lactone (AHL) synthase and a corresponding cognate receptor, play roles in synthesizing and sensing autoinducers, respectively (Miller & Bassler, 2001). The LuxR–LuxI QS system from *Vibrio fischeri* has been intensively studied as the first model of cell-density-dependent gene regulation (Nealson & Hastings, 1979; Nasser & Reverchon, 2007). Subsequent studies on LuxR and LuxI homologues identified in other bacterial species revealed the biochemical mechanism of the LuxR–LuxI QS system: a LuxI homologue synthesizes autoinducers (acyl-homoserine

lactones), which freely diffuse out of the cell membrane, while a LuxR homologue is a transcription factor whose activity is regulated in response to the binding of a specific autoinducer. The lengths of the acyl moieties of the AHL molecules can vary between four and 18 C atoms, and the third C atom in the acyl chain can be either a carbonyl group, a hydroxyl group or a methylene moiety (Whitehead *et al.*, 2001; Marketon *et al.*, 2002). These structural differences in the AHLs play a crucial role in the signalling specificity of QS receptors in different bacterial species.

Although a large number of putative LuxR–LuxI pair homologues have been identified in Gram-negative bacteria (Fuqua *et al.*, 1996), the LuxR–LuxI-type QS system in *Escherichia coli* is poorly characterized. *E. coli* possesses a LuxR homologue named SdiA (**s**uppressor of cell **di**vision **i**nhibitor), which exhibits sequence similarity to the LuxR-type transcription factors (Fig. 1), but this bacterium lacks a gene encoding a LuxI homologue. Originally, SdiA was identified as a transcriptional activator of the *ftsQAZ* operon that encodes essential cell-division proteins (Wang *et al.*, 1991). Further evidence suggests that it also participates in the regulation of genes involved in various cellular activities such as metabolism, motility, virulence, survival and defence mechanisms (Kanamaru *et al.*, 2000; Wei *et al.*, 2001; Rahmati *et al.*, 2002; Van Houdt *et al.*, 2006; Lee *et al.*, 2007). The role of SdiA as a LuxR-type QS receptor has been clarified through its abilities to respond to synthetic AHLs (Van Houdt *et al.*, 2006) or AHLs exclusively emanating from other bacterial species (Smith *et al.*, 2008; Hughes *et al.*, 2010). Despite the absence of an autoinducer synthase homologue in *E. coli*, a compound produced by *E. coli* itself was proposed to influence the transcriptional activity of SdiA towards the P2 promoter of the *ftsQ* gene (Sitnikov *et al.*, 1996). In this regard, indole was proposed as an SdiA-mediated interspecies biofilm signal or an inhibitory factor in the AHL response of SdiA (Lee *et al.*, 2007; Sabag-Daigle *et al.*, 2012). These findings suggest that

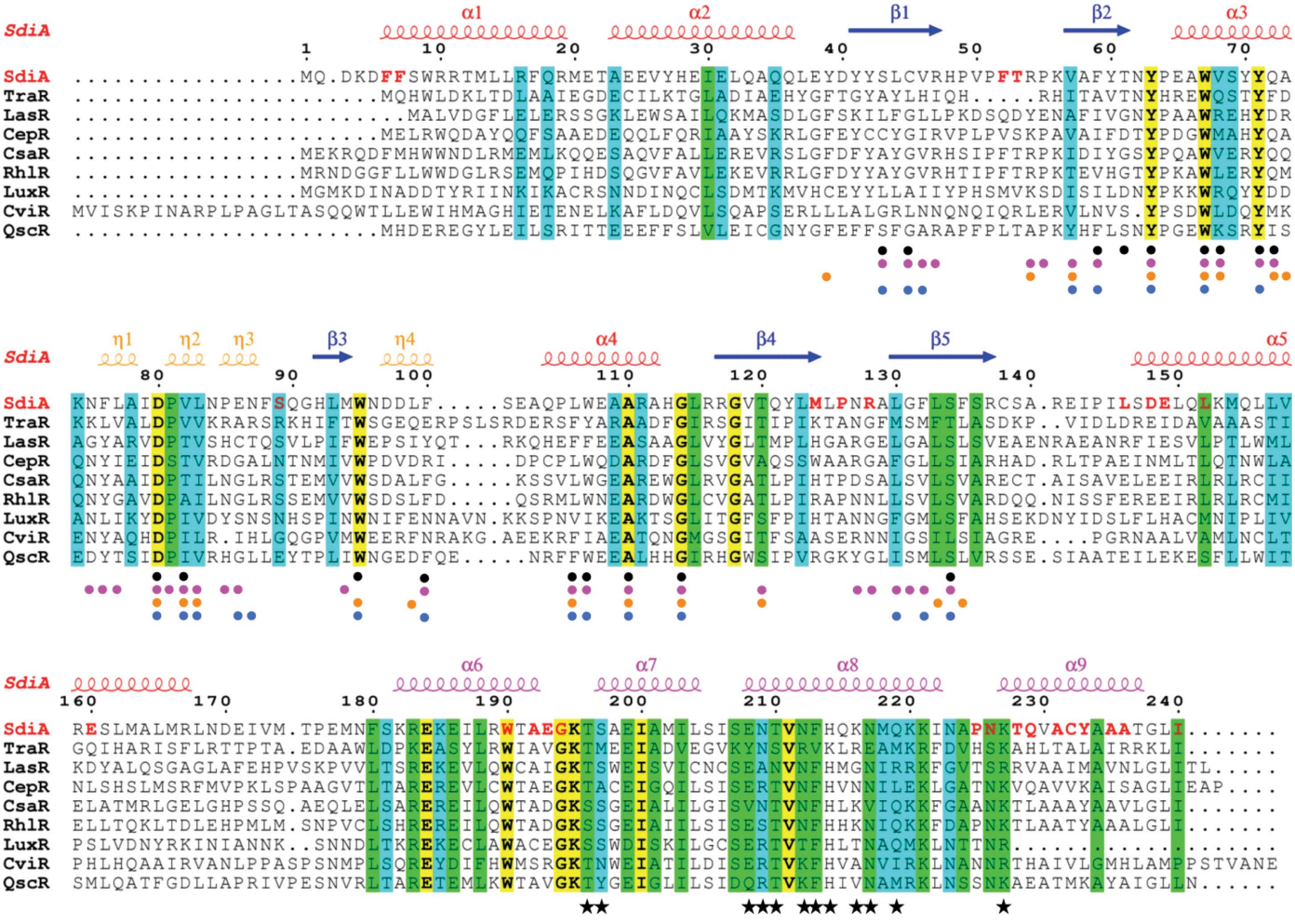

Figure 1
Multiple sequence alignment of SdiA and its homologues. The protein sequences are for *E. coli* SdiA (UniProt P07026), *A. tumefaciens* TraR (UniProt A5WYC9), *P. aeruginosa* LasR (UniProt P25084), *Burkholderia cepacia* CepR (UniProt Q9ZIU0), *P. chlororaphis* CsaR (UniProt Q939D1), *P. aeruginosa* RhlR (UniProt B6E4Z5), *V. fischeri* LuxR (UniProt Q6WEK4), *C. violaceum* CviR (UniProt D3W065) and *P. aeruginosa* QscR (UniProt G3XD77). Identical residues are boxed in yellow. Green and cyan boxes depict significantly and weakly conserved residues, respectively. Secondary structures and residue numbering of SdiA are shown above the alignment. The residues involved in ligand and DNA binding in TraR are denoted by black dots and stars, respectively. The residues involved in ligand binding in LasR, CviR and QscR are denoted by pink, orange and blue dots, respectively. The residues mostly involved in the dimerization of SdiA are emphasized by a red colour.

SdiA possesses a complicated mechanism for recognizing diverse ligands and conducting cell signalling that differs from those of other QS receptors. Therefore, the *E. coli* QS receptor SdiA seems to bridge both intraspecies and interspecies communication.

In most cases, recombinant QS receptors can only be expressed and prepared in a soluble form in the presence of the corresponding AHL molecules (Zhu & Winans, 1999, 2001; Yao *et al.*, 2006; Bottomley *et al.*, 2007), possibly owing to the instability of the QS receptor in the absence of autoinducers. Accordingly, all structures of QS receptors reported to date have been determined in complexes with AHL molecules, including the crystal structures of intact *Agrobacterium tumefaciens* TraR (Vannini *et al.*, 2002; Zhang *et al.*, 2002), *Chromobacterium violaceum* CviR (Chen *et al.*, 2011), *Pseudomonas aeruginosa* QscR (Lintz *et al.*, 2011), the ligand-binding domain (LBD) of *P. aeruginosa* LasR (Bottomley *et al.*, 2007) and the solution structure of the LBD of *E. coli* SdiA (Yao *et al.*, 2006). AHL has been proposed to enhance proper folding of the QS receptor (Chai & Winans, 2005; Yao *et al.*, 2006; Bottomley *et al.*, 2007). However, such a role of AHL has not been experimentally proven owing to difficulty in preparing the apo receptors.

QS receptors are considered to be potential targets for the development of novel compounds against pathogenic bacteria (Rasmussen & Givskov, 2006; Skilbeck *et al.*, 2009). In particular, owing to the involvement of SdiA in controlling virulence factors and multidrug efflux pumps in enterohaemorrhagic *E. coli* O157:H7 and *Salmonella typhimurium* (Ahmer *et al.*, 1998; Rahmati *et al.*, 2002; Sperandio, 2010), various efforts to develop chemical inhibitors targeting SdiA have been reported (Ravichandiran *et al.*, 2012). The high-resolution structures of intact SdiA are especially important in this context since the atomic architectures of the ligand-bound complexes will serve as valuable scaffolds for the rational design of drug candidates (Galloway *et al.*, 2011, 2012).

In this study, we report crystal structures of intact SdiA, and with the ability to prepare apo SdiA on a large scale we also provide biochemical data that explain the ligand specificity of SdiA for various AHLs. In addition, based on these analyses, we propose that the transcriptional activity of SdiA might be affected not only by quorum signals but also by other environmental factors such as oxidation.

2. Materials and methods

2.1. Materials

All chemicals used in this study were purchased from Sigma (St Louis, Missouri, USA) unless specified otherwise. The primers used in this study were synthesized by Bioneer Corporation, Republic of Korea and are listed in Supplementary Table S3.[1] The atomic coordinates of TraR and LasR with PDB entries 1l3l (Zhang *et al.*, 2002) and 2uv0 (Bottomley *et al.*, 2007), respectively, were used for structural comparison.

2.2. Protein preparation and crystallization

Protein expression and preparation have been described previously (Wu *et al.*, 2008). Briefly, selenomethionine-substituted (SeMet) protein was expressed in *E. coli* B834 (DE3) cells (Novagen, USA), a methionine-auxotroph strain. Cells were grown at 310 K in M9 medium supplemented with 50 µg ml^{-1} ampicillin and 100 µg ml^{-1} L-selenomethionine until the OD_{600} reached 0.6. The culture temperature was then decreased to 303 K and isopropyl β-D-1-thiogalactopyranoside (IPTG) was added to a final concentration of 0.1 m*M* to induce protein expression. After 4 h, the cell pellets were harvested by centrifugation at 6500*g* for 10 min at 277 K and stored at 253 K until use. SeMet SdiA was purified in the presence of PEG 3350 as a stabilizer and was crystallized using the same procedure as used for the native form (Wu *et al.*, 2008). The native protein was also prepared in the absence of stabilizer for subsequent biochemical analyses by modifying the previous purification method (Wu *et al.*, 2008). For the preparation of apo SdiA, after the immobilized metal-affinity chromatography step the elution fractions were pooled and diluted five times in pre-chilled loading buffer (25 m*M* HEPES pH 7.5, 100 m*M* NaCl, 5 m*M* DTT). The protein solution was loaded onto a HiTrap Heparin column (GE Healthcare, Sweden) and the column was washed intensively with loading buffer containing 200 m*M* NaCl. Finally, the SdiA protein was eluted from the column with loading buffer containing 1 *M* NaCl. The protein solution was concentrated, flash-frozen and stored at 193 K until use. Both hexagonal and monoclinic crystals were obtained from conditions containing 100 m*M* HEPES pH 7.2, 200 m*M* Li_2SO_4 and 4.6 mg ml^{-1} protein by the hanging-drop vapour-diffusion method at 287 K.

2.3. Data collection and structure determination

Three-wavelength anomalous diffraction data sets were collected from a monoclinic crystal of SeMet SdiA to 2.4 Å resolution on beamline 6B of the Pohang Accelerator Laboratory (PAL), Republic of Korea. Native data sets from monoclinic and hexagonal crystals were collected to 2.26 and 2.7 Å resolution, respectively, on beamline 41XU of the Spring-8 synchrotron, Japan. All diffraction data were processed and scaled using the *HKL*-2000 program package (Otwinowski & Minor, 1997). The unit-cell parameters of the crystal belonging to the monoclinic space group *C*2 were $a = 96.28$, $b = 68.69$, $c = 69.28$ Å, $\beta = 126.47^\circ$, while those of the crystal belonging to the hexagonal space group $P6_522$ were $a = b = 130.47$, $c = 125.23$ Å. The structure of SdiA in space group *C*2 was determined using the multiple-wavelength anomalous diffraction (MAD) method. The positions of three selenium sites in SdiA were identified using *SOLVE* (Terwilliger & Berendzen, 1999). Subsequently, an initial phase was calculated and an initial model was built using *RESOLVE* (Terwilliger, 2000, 2003). Manual model building was

[1] Supporting information has been deposited in the IUCr electronic archive (Reference: LV5056).

continuously performed with *O* (Jones *et al.*, 1991) and the models were refined using the *CNS* program suite (Brünger *et al.*, 1998). The structures of native SdiA in space groups *C*2 and $P6_522$ were solved by molecular replacement using *MOLREP* (Vagin & Teplyakov, 2010) with the SeMet SdiA structure as a template. During the final stages of model refinement, atomic positions and isotropic *B* factors were refined using *REFMAC*5 (Murshudov *et al.*, 2011). The qualities of the final structures were validated using *PROCHECK* (Laskowski *et al.*, 1993). The Ramachandran plot of the SdiA model reveals that it has a good geometry, with no residues in disallowed regions. The data-collection and refinement statistics are summarized in Table 1. Structural representations were prepared using *PyMOL* (v.1.5.0.4; Schrödinger) or *VMD* (Humphrey *et al.*, 1996).

In this study, the *C*2 structure was used for structural analyses unless otherwise specified. There is one molecule in the asymmetric unit of both crystal forms. The first four N-terminal residues and the C-terminal His_6 tag (LEHHHHHH) were disordered and were not included in the final model. Therefore, 236 residues (residues 5–240) are modelled in the current *E. coli* SdiA structures.

Table 1
Data-collection and refinement statistics.

Values in parentheses are for the highest resolution shell.

	SeMet SdiA				
	Peak	Inflection	Remote	Native SdiA	
Data collection					
Space group	*C*2			*C*2	$P6_522$
Wavelength (Å)	0.9793	0.9795	0.9717	1.0000	1.0000
Unit-cell parameters					
a (Å)	96.17	96.25	96.31	96.28	130.47
b (Å)	68.00	68.08	68.16	68.69	130.47
c (Å)	69.25	69.29	69.31	69.28	125.23
β (°)	126.18	126.18	126.20	126.47	90.00
Resolution range (Å)	30–2.4	30–2.4	30–2.5	30–2.26	30–2.7
Total reflections	85605 (7528)	83165 (6288)	74944 (5718)	51012 (2882)	180341 (17605)
Unique reflections	14206 (1394)	14141 (1310)	12511 (1167)	16343 (1310)	17821 (1726)
Multiplicity	6.0 (5.4)	5.9 (4.8)	6.0 (4.9)	3.1 (2.2)	10.1 (10.2)
$\langle I/\sigma(I)\rangle$	26.5 (3.6)	26.4 (3.1)	28.8 (2.8)	14.7 (2.0)	41.9 (5.5)
Completeness (%)	99.3 (97.7)	98.4 (92.4)	98.7 (93.7)	95.9 (78.1)	99.8 (100)
R_{merge}† (%)	9.9 (34.5)	7.7 (36.9)	7.6 (41.8)	7.3 (34.0)	5.8 (39.8)
MAD phasing					
Resolution range (Å)		30–2.4			
No. of methionine residues		3			
No. of heavy-atom sites found		3			
FOM‡		0.48			
Solvent-flattening FOM‡		0.63			
Refinement					
Resolution (Å)				30–2.26	30–2.70
Reflections used (working/free)				15523/819	16858/902
R_{work}/R_{free}§ (%)				21.3/27.6	23.0/27.1
Average *B* factor, all atoms (Å^2)				35.7	56.1
No. of protein molecules in asymmetric unit				1	1
R.m.s.d. from ideal					
Bond lengths (Å)				0.013	0.013
Bond angles (°)				1.411	1.51
Ramachandran plot (%)					
Most favoured				94.9	92.2
Additionally allowed				5.1	7.8
Generously allowed				0	0
Disallowed				0	0

† $R_{merge} = \sum_{hkl}\sum_i |I_i(hkl) - \langle I(hkl)\rangle| / \sum_{hkl}\sum_i I_i(hkl)$, where $I_i(hkl)$ is the observed intensity and $\langle I(hkl)\rangle$ is the average intensity for multiple measurements. ‡ These values are from the outputs of *SOLVE* and *RESOLVE*. § *R* factor = $\sum_{hkl} ||F_{obs}| - |F_{calc}|| / \sum_{hkl} |F_{obs}|$.

2.4. Site-directed mutagenesis

The Cys45 and Cys138 residues in the LBD and the Cys232 residue in the DBD of SdiA were individually substituted by serine using the QuikChange Site-Directed Mutagenesis Kit (Agilent Technologies, USA) according to the manufacturer's manual. The primers are listed in Supplementary Table S3. The mutant proteins were expressed and purified in the same way as for wild-type SdiA.

2.5. Isothermal titration calorimetry (ITC) measurements

Binding between SdiA and AHLs with various acyl chain lengths was measured using a VP-ITC microcalorimeter (MicroCal, USA) with a reaction cell volume of 1.4 ml. SdiA was dialyzed against ITC buffer (25 m*M* HEPES pH 7.5, 1 *M* NaCl, 0.5 m*M* DTT, 1.8% DMSO) at 277 K overnight. In a typical binding experiment, the cell contained 78 µ*M* SdiA stirred at 300 rev min^{-1} and the syringe contained 1.8 m*M* AHL. A titration experiment consisted of 25–30 injections of 10 µl at 4 min intervals with the chamber maintained at 298 K. For calculation of the binding constant (K_d), a nonlinear least-squares regression curve was fitted to the data with the *Origin* v.5.0 software (MicroCal, USA) using one-site or two-site binding models.

2.6. Circular-dichroism (CD) measurements

The secondary structures of wild-type and mutant SdiA were examined by monitoring the far-UV CD spectra (200–260 nm). CD measurements were conducted with 1 mg ml^{-1} protein in CD buffer (50 m*M* sodium phosphate pH 7.4, 0.25 *M* NaCl, 2 m*M* DTT) in a 1 mm quartz cell. CD spectra were obtained using a Jasco J-810 spectropolarimeter (Jasco, Japan) and were processed using the *Spectra Manager* software (Jasco, USA). Each spectrum was displayed as an average of triplicate measurements. The thermal stabilities of SdiA in various conditions were evaluated by monitoring

its ellipticity changes at 220 nm from 283 to 363 K. Melting temperatures (T_m) were calculated as described by Greenfield (2007) using *SigmaPlot* (Systat Software Inc., USA) and are summarized in Fig. 5(*c*).

2.7. Dimerization assay

To confirm the oxidation-dependent dimerization of SdiA, the proteins were oxidized using H_2O_2/NaI by incubation in a reaction mixture consisting of 100 m*M* NH_4HCO_3, 1 *M* NaCl at 303 K for 30 min with a shaking speed of 500 rev min^{-1}. Subsequently, protein solutions were analyzed by nonreducing SDS–PAGE followed by Coomassie Brilliant Blue staining.

2.8. Western blot analyses

The wild-type and mutant SdiA were expressed in *E. coli* BL21 (DE3) cells in 5 ml Luria–Bertani (LB) broth under the same culture and expression conditions as described above, except that the cells were cultured at 291 K for 24 h after IPTG induction. Cells at the same OD_{600} were harvested by centrifugation and resuspended in 0.5 ml phosphate-buffered saline (PBS). After sonication on ice, the supernatant was collected by centrifugation at 10 000*g* for 20 min at 277 K and was mixed with 2× Laemmli sample buffer without reducing agent for SDS–PAGE. After electrophoresis in a Tris–glycine gel, proteins were transferred onto a Protran Nitrocellulose Membrane (Whatman, Germany) using a Mini Trans-Blot cell (Bio-Rad, USA) following the manufacturer's instructions. The membrane was then washed several times with PBS buffer containing 0.05% Tween 20 (PBS-T) and was subsequently blocked with 5% skimmed milk in PBS-T at room temperature for 1 h. For specific antigen detection, the blocked membrane was incubated with mouse monoclonal anti-His_6 antibodies (IG Therapy Co., Republic of Korea) diluted 1700-fold in PBS-T for 1 h. In the final step, the membrane was incubated with goat anti-mouse IgG-HRP (Santa Cruz Biotechnology, USA) diluted 2500-fold in PBS-T for a further 1 h. For signal detection, the membrane was incubated in pico EPD (Elpis Biotech. Inc., Republic of Korea), a highly enhanced peroxidase detection solution, for 3 min prior to X-ray film exposure (AGFA Healthcare, Belgium). Finally, the film was developed using a JP-33 automatic X-ray film processor (JPI, Republic of Korea).

2.9. Gel-shift assay

The 339 bp *uvrY* promoter was amplified by polymerase chain reaction using the primer pair *uvrY*-pro-F and *uvrY*-pro-R (Supplementary Table S3) with *E. coli* genomic DNA as a template. Two complementary oligonucleotides (*ftsQ*P2-F and *ftsQ*P2-R; Supplementary Table S3) with the sequence of the *ftsQ*P2 promoter (Yamamoto *et al.*, 2001) were synthesized, mixed in an equal molar ratio and annealed. Double-stranded *ftsQ*P2 promoter was purified using a Mono Q 4.6/100 PE column (GE Healthcare, Sweden) and desalted in a buffer consisting of 25 m*M* Tris–HCl pH 7.5, 50 m*M* NaCl using illustra NAP-5 columns (GE Healthcare, Sweden). The DNA products were end-labelled with (γ-^{32}P)-ATP (GE Healthcare, USA) using T4 polynucleotide kinase (New England BioLabs Inc., USA). The unincorporated isotope-labelled ATPs were removed using PROBER, a probe DNA-purifying system (iNtRON Biotechnology, Republic of Korea). After incubation of DNA and protein in DNA-binding buffer [25 m*M* Tris–HCl pH 7.5, 50 m*M* NaCl, 1 m*M* $MgCl_2$, 0.5 m*M* DTT, 2 µg poly(G–C) DNA, 5% glycerol] for 30 min at 303 K, the samples were separated on 6% polyacrylamide gels, which were pre-run at 100 V for 1 h at 277 K.

Electrophoresis was conducted at room temperature using 0.5× TGE

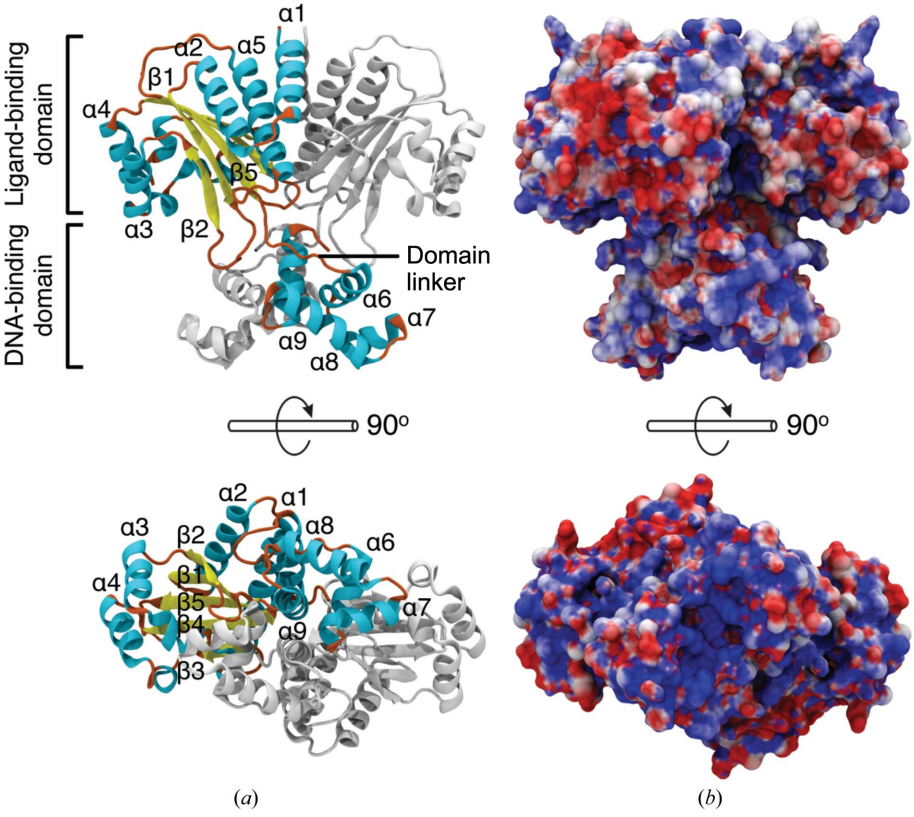

Figure 2
Overall structure of the SdiA dimer. (*a*) Ribbon diagrams of the SdiA dimer are drawn in two different views. Secondary-structure elements in one monomer are labelled and indicated in different colours: α-helices and 3_{10}-helices are coloured cyan and β-strands and loops are coloured yellow and orange, respectively. The other monomer is drawn in grey. (*b*) Charge-distributed surface models of dimeric SdiA ($\pm 5kT\ e^{-1}$) in the same orientation as in (*a*). The red and blue colours represent negatively and positively charged surfaces, respectively. A plausible DNA-binding pocket with positively charged surfaces is located at the bottom of the C-terminal domain.

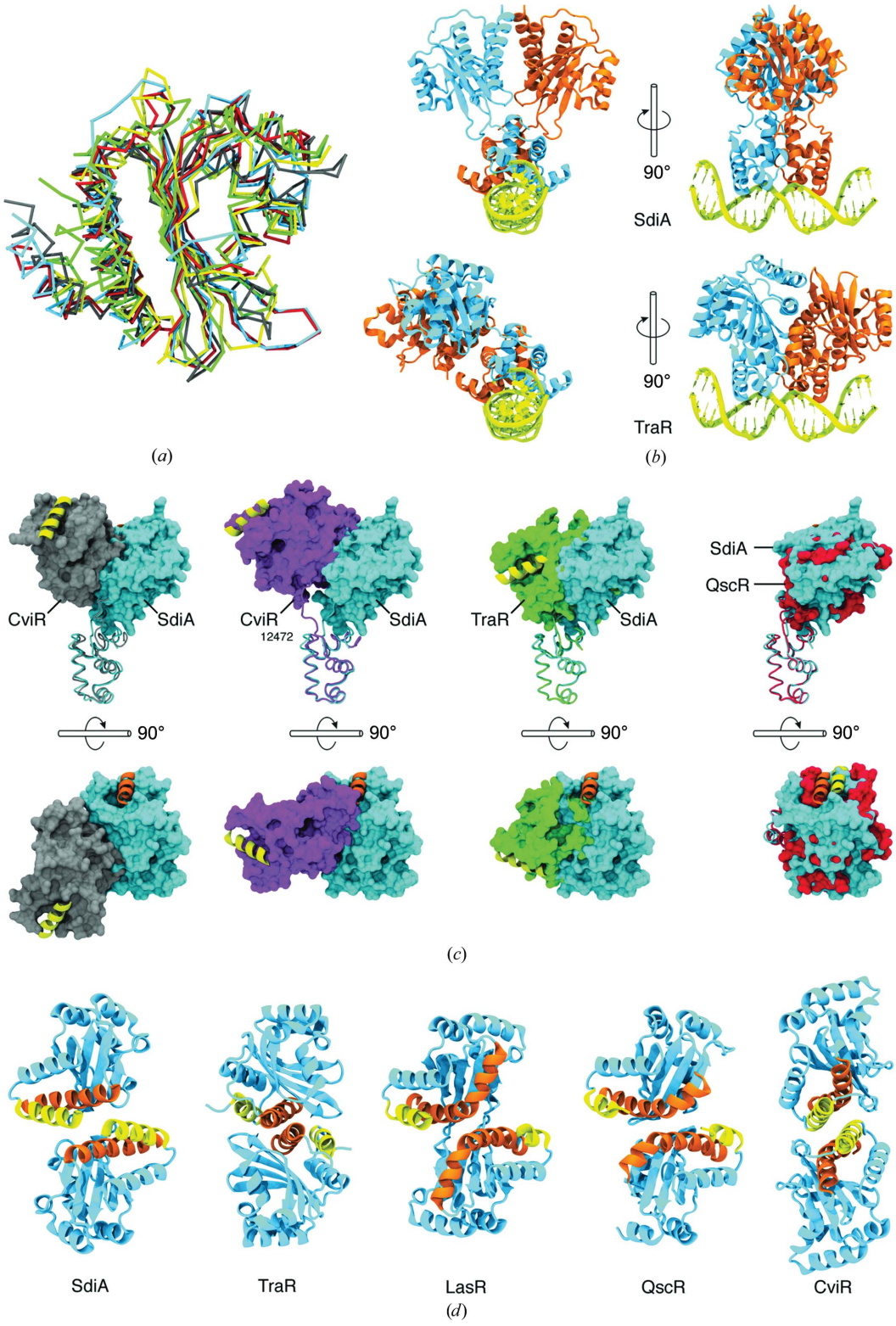

Figure 3
Structural comparison of SdiA with its homologues. (*a*) The backbone traces of the N-terminal LBDs of SdiA (cyan), TraR (green), CviR (PDB entry 3qp2; grey; Chen *et al.*, 2011), LasR (yellow) and QscR (red) are overlapped for structural comparison. (*b*) Predicted DNA-binding model of SdiA (top) and its comparison with the TraR–DNA complex (bottom) in two orientations rotated clockwise by 90°. The DNA molecules are coloured yellow, and the protein monomer subunits are illustrated as cyan and orange ribbon diagrams. (*c*) Structural superimpositions of SdiA (cyan) with CviR (PDB entry 3qp5; grey), $CviR_{12472}$ (PDB entry 3qp6; magenta), TraR (green) and QscR (red) in two different orientations. The C-terminal DBDs presented by the backbone traces were used for the structural overlap, and the N-terminal LBDs are presented as surface-filling models. The helix α4 of SdiA (orange) and equivalent α-helices in SdiA homologues (yellow) were used as references. (*d*) Comparison of the dimeric LBDs of SdiA, TraR, LasR, QscR and CviR (PDB entry 3qp2). Each ribbon model is shown along the twofold axis. The α1 helices are coloured yellow, while helix α5 of SdiA and equivalent helices in other receptors are shown in orange.

buffer (25 m*M* Tris, 190 m*M* glycine, 1 m*M* EDTA) at 100 V for 50 min for the *ftsQ*P2 promoter or 2 h for the *uvrY* promoter. Gels were dried on 3MM Chr blotting papers (Whatman, England) at 353 K for 30 min and radioactive bands were visualized by autoradiography after incubation at 203 K for 12 h.

3. Results

3.1. Overall structure of *E. coli* SdiA

The crystal structure of *E. coli* SdiA was determined in two different space groups, *C*2 and $P6_522$, at 2.26 and 2.70 Å resolution, respectively. In the description of the subsequent structural analyses, the SdiA structure in space group *C*2 is used unless specified otherwise. This crystal structure revealed that SdiA is composed of two domains, an N-terminal ligand-binding domain (LBD; residues 5–167) and a C-terminal DNA-binding domain (DBD; residues 184–240), which are connected by a linker (residues 168–183) (Fig. 2*a*). The LBD is composed of a central antiparallel five-stranded β-sheet surrounded by α-helices on each side, generating an $\alpha/\beta/\alpha$ topology. A ligand-binding site is located on a concave surface of the β-sheet. The DBD comprises four α-helices, of which helices α8 and α9 form a typical helix–turn–helix DNA-binding motif (Fig. 2*a*). Although the LBD of SdiA exists as a monomer in solution (Yao *et al.*, 2006), full-length SdiA is required to be dimeric for its DNA-binding activity. As confirmed by size-exclusion chromatography, purified intact SdiA exists as a dimer in solution (Supplementary Fig. S1). Accordingly, an SdiA dimer was built using a crystallographic twofold symmetry operation (Fig. 2). The dimer interface of SdiA is mostly hydrophobic, with buried surfaces of 800 and 551 Å^2 for the LBD and DBD, respectively. Helices α1 and α5 in the LBD and helices α6 and α9 in the DBD mostly contribute to the intersubunit interaction (Fig. 2 and Supplementary Table S1).

3.2. Structural comparison with LuxR homologues

The current crystal structures of SdiA exhibit a similar fold to the mean NMR structure of the SdiA LBD (Yao *et al.*, 2006) with a root-mean-square deviation (r.m.s.d.) of 2.4 Å (Supplementary Fig. S2). In addition, the overall fold of the

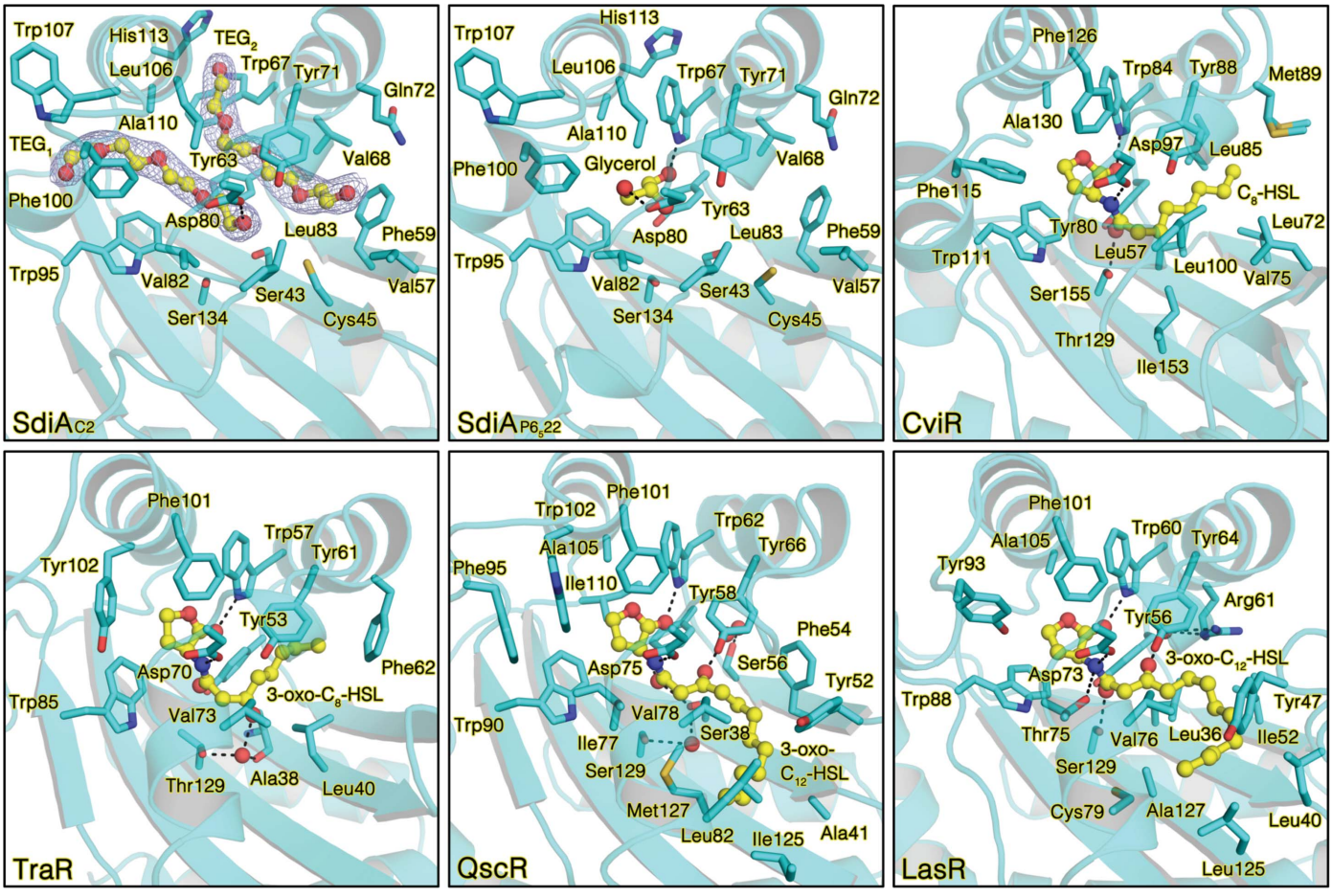

Figure 4
Structural comparison of the ligand-binding sites of SdiA and its homologues. Ligands are represented as yellow ball-and-stick models, and residues involved in ligand interaction are shown as stick models. Water molecules are depicted as red spheres and hydrogen bonds are illustrated as black dotted lines. Electron-density maps of TEGs in the SdiA structure are contoured at the 1.0σ level.

core of the SdiA LBD is similar to those of other known LuxR-type QS receptors, including TraR, LasR, CviR and QscR (Fig. 3*a* and Supplementary Table S2), even though their sequence identity is not high (Fig. 1). In contrast to the LBD, the SdiA DBD is relatively similar to those in other receptors in terms of both sequence (Fig. 1) and fold (Fig. 3*c* and Supplementary Table S2). However, despite the folding similarity of the LBDs and DBDs, the relative orientations of these two domains are different in the LuxR-type receptors (Fig. 3*c*). When structural superimposition is applied to the DBDs, the LBDs of TraR/CviR$_{12472}$ and CviR are rotated approximately 90° and 180° from that of SdiA along the axis near the linker, respectively, whereas the QscR LBD superimposes well on that of SdiA (Fig. 3*c*). The residues involved in interdomain interactions are also dissimilar, implying that the interdomain contact is not conserved in the LuxR-type QS receptors.

Structural differences are also noted in the dimeric interface of the LBDs (Fig. 3*d*). In TraR, QscR and LasR, the LBDs dimerize mostly through helix α6, which is the longest helix, connecting the LBDs and DBDs. In CviR, helix α1 plays a major role in dimer formation, while in SdiA helix α1 of one subunit interacts with helix α5 of the other subunit in the dimeric interface (see Supplementary Table S1). Furthermore, the subunit interaction of SdiA through these helices is not as tight as those in other receptors, making the dimeric SdiA LBD unique among the current reported structures of the LuxR-type receptors and to some extent explaining why the SdiA LBD exists as a monomer in solution (Yao *et al.*, 2006). Accordingly, the dimerization interfaces of the LBDs are 800, 487, 970, 1266 and 1578 Å^2 for SdiA, QscR, TraR, LasR and CviR, respectively, suggesting a diverse quaternary architecture of the QS receptors, although their overall structures as monomers are quite well conserved.

3.3. A preformed wide and open ligand-binding pocket

Even though the crystals of intact SdiA were grown in the absence of AHLs, two baguette-shaped electron densities nearly parallel to each other were identified in the ligand-binding pocket of SdiA (Fig. 4). Considering the materials used in crystallization, it was expected that low-molecular-weight PEG present in the PEG 3350 used as a stabilizer during purification and crystallization had been captured in the ligand-binding site. Accordingly, four units of ethylene glycol (tetraethylene glycol; TEG) were modelled into the extra densities with good geometry (Fig. 4). Similar to the ligand–receptor interactions found in other QS receptors, two TEG molecules (TEG-1 and TEG-2) form a wide hydrophobic interaction with the residues in the ligand-binding pocket of SdiA. TEG-1 is located in a pocket lined by the side chains of Ser43, Trp95, Phe100, Leu106, Trp107, Ala110 and Arg116, while TEG-2 is located in a pocket lined by the side chains of Phe59, Tyr63 and Tyr71 (Fig. 4; see also Supplementary Fig. S4). Among these residues, Tyr63, Tyr71, Trp95 and Ala110 are strictly conversed in the LuxR-type receptors (Fig. 1), whereas the others are not conserved, although their equivalents in TraR, LasR, QscR and CviR are involved in AHL binding (Fig. 4). A hydrogen bond between the O$^{\delta1}$ atom of Asp80 and the O5 atom of TEG-1 also contributes to the SdiA–TEG interaction (Fig. 4). The most important difference between SdiA and other receptors is the size and the shape of the ligand-binding pocket. While the AHLs bound to TraR, LasR, QscR and CviR are completely embedded in an enclosed cavity with limited solvent contact, the ligand-binding pocket of SdiA is wide open to the solvent (Supplementary Fig. S3). In addition, the size of the binding pocket of SdiA is almost twice those of other receptors (Supplementary Fig. S3). The wide and open ligand-binding pocket of SdiA is likely to accommodate various autoinducers, partially explaining the broad ligand selectivity of SdiA.

Interestingly, although the same protein was used for crystallization of the *C*2 and $P6_522$ crystals, no electron density corresponding to TEG was found in the $P6_522$ structure. Instead, an electron density fitted by a glycerol molecule was observed (Fig. 4). Since the glycerol molecule is much smaller than the AHL or TEG molecules, it has minimal binding to protein residues. Indeed, in the $P6_522$ crystal structure the glycerol molecule forms hydrogen bonds to the side chains of Asp80 and Trp67 (Fig. 4). It is worth noting that these two residues are strictly conserved in the LuxR-type receptors (Fig. 1) and all of their equivalents contribute to the interactions between the LBDs and the lactone moiety of AHLs (Fig. 4). Surprisingly, there is no overall structural difference between the *C*2 and $P6_522$ structure forms; superimposition of the LBDs and intact proteins gives r.m.s.d.s of 0.52 and 0.62 Å over 160 and 232 C$^\alpha$ atoms, respectively (see also Supplementary Fig. S2). However, ligand binding seems to cause a local conformation change near the ligand-binding sites: His113 is shifted outwards along helix α4 by approximately 2 Å and the Trp67 side chain is swung outwards, synergistically allowing the TEG-2 molecule to be accommodated in the ligand-binding site (Supplementary Fig. S4). In addition, most residues in the ligand-binding pockets in the crystal structures overlap with those in the solution structure, except for Trp67, Leu83 and Trp107 owing to their interaction with the ligand or a stabilizer. Collectively, these findings suggest that the ligand-binding pocket might be preformed and that ligand binding might not cause any conformational change in the overall fold.

3.4. Binding selectivity for short acyl-chain ligands

In the crystal structure of *C. violaceum* CviR, Met89 was proposed to be essential for determining the AHL length selectivity of CviR (Chen *et al.*, 2011). Similarly, Phe62 of TraR, located in the equivalent position to Met89 of CviR (Fig. 4), was also thought to play an occlusive role by preventing access of the solvent to the acyl tail of its ligand (Vannini *et al.*, 2002; Zhang *et al.*, 2002). Structural alignment of SdiA with CviR in various ligand-bound forms revealed that Gln72 and Phe59 of SdiA could perform a similar role to that of Met89 of CviR (Fig. 5*b*), restraining the length of the acyl chain. From this analysis, it is predicted that SdiA cannot accommodate AHLs with chain lengths longer than eight C

atoms (Fig. 5*b*). Further supporting this hypothesis, isothermal titration calorimetric (ITC) measurements were performed to investigate the interaction between SdiA and AHLs with various acyl-chain lengths (Fig. 5*a*). To avoid a competition effect of the stabilizer (*e.g.* PEG) in biochemical assays, SdiA protein was purified in the absence of any stabilizer in an attempt to obtain the apo form (see §2). In agreement with the structure-based prediction, SdiA showed binding to C_4-HSL and C_8-HSL with K_d values of 7.0 ± 0.8 μ*M* and 36.7 ± 10.9 n*M*, respectively. However, no heat was released by the titration of C_{10}-HSL; this might be owing to the poor solubility of C_{10}-HSL, because a high concentration of C_{10}-HSL was used for the ITC experiment. To further clarify the ligand selectivity of SdiA, the protein was subjected to thermal stability measurement with AHLs. Consistent with the ITC results, C_8-HSL exhibited the most prominent effect on the stability of SdiA, with a melting temperature (T_m) of 335.17 ± 0.16 K compared with the T_m values of 327.46 ± 0.05 and

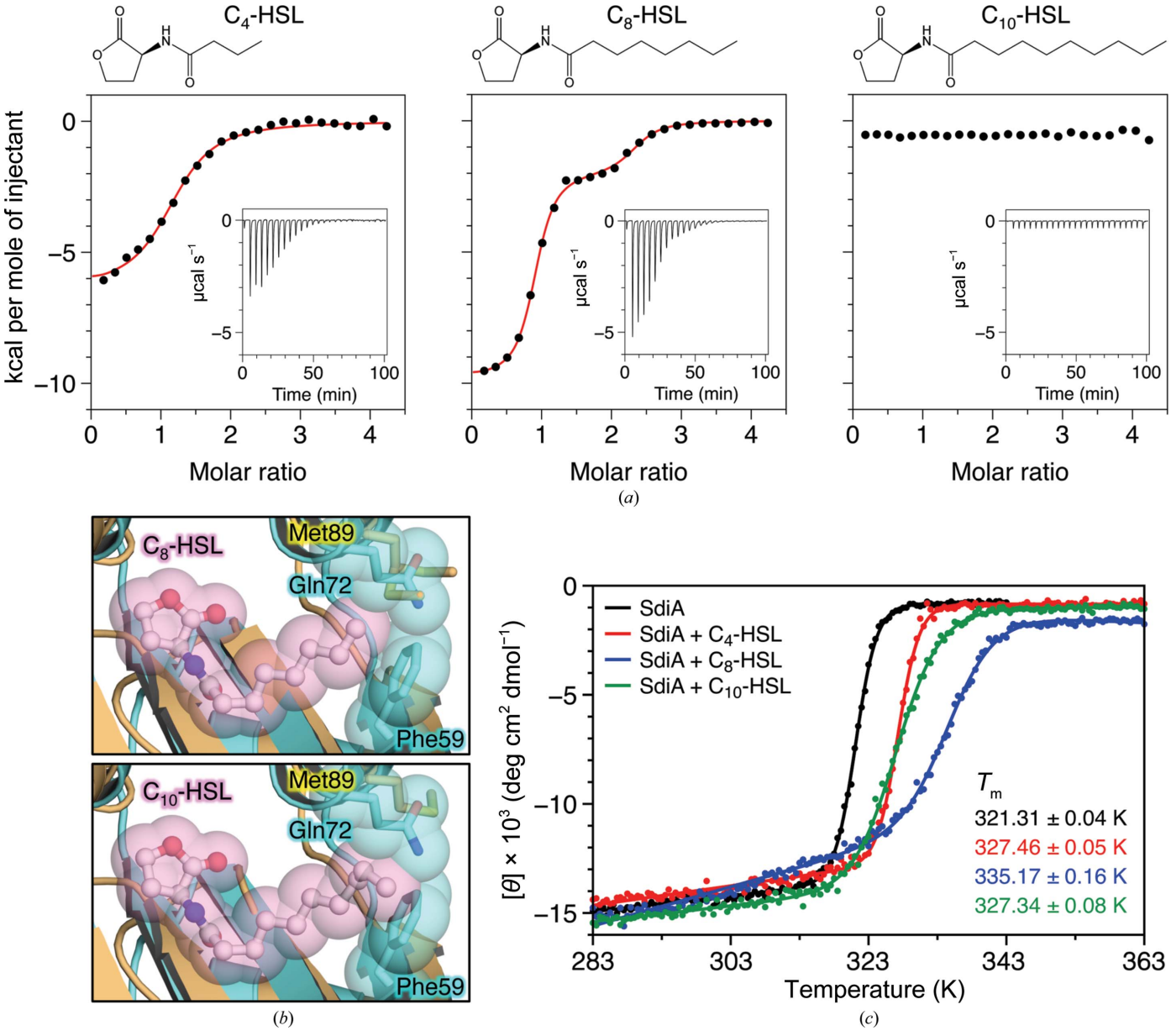

Figure 5
Ligand specificity of SdiA. (*a*) ITC analyses of different AHLs (drawn at the top) titrated against purified SdiA. The integrated heat exchanges measured at each injection are shown, and the raw data are presented in the inset. The red lines represent nonlinear least-squares data fitting. (*b*) Structural comparison of the ligand-binding sites of SdiA (cyan) and CviR (orange) in complex with C_8-HSL (PDB entry 3qp2; left) or C_{10}-HSL (PDB entry 3qp4; right). AHLs are illustrated as white ball-and-stick models covered by transparent pink spheres. The side chains of the occlusive residues Phe59 and Gln72 of SdiA and Met89 of CviR are shown as stick models. (*c*) Thermal stability of SdiA in the presence of different AHLs. The ellipticity changes at 220 nm were monitored from 283 to 343 K and from 283 to 363 K in the absence and presence of AHLs, respectively. The dots represent the raw data and the solid lines depict the fitted curve to calculate the melting temperatures (T_m) that are shown in the lower right corner. Data are represented as mean ± standard error.

327.34 ± 0.08 K for C_4-HSL and C_{10}-HSL, respectively (Fig. 5*c*). These results, combined with the ITC observations, indicate that the binding of C_8-HSL to SdiA is stronger than that of C_4-HSL and C_{10}-HSL.

3.5. Cys232 in the SdiA DBD is involved in intersubunit disulfide-bond formation

Electrostatic potential surface analysis reveals that the bottom of the C-terminal domains of dimeric SdiA forms a positively charged concave surface that possibly fits into the double-stranded DNA (Fig. 2*b*). To elucidate the DNA-binding mode of SdiA, a model structure of SdiA bound to double-stranded DNA was created by overlapping the dimeric DBD of *E. coli* SdiA onto that of an *A. tumefaciens* TraR dimer (PDB entry 1l3l; Zhang *et al.*, 2002) followed by energy minimization using the *CNS* program (Fig. 3*b*). The SdiA–DNA model suggests that each SdiA monomer interacts with the major groove of DNA primarily through residues from helix α8 (Fig. 3*b*), suggesting that SdiA shares a similar DNA-binding mode with other LuxR-type QS receptors. However, some putative binding residues are not strictly conserved in the LuxR homologues (*e.g.* Asn209 and Lys216; Fig. 1), explaining the binding specificity of each AHL receptor for its cognate DNA promoters. SdiA is known to recognize an SdiA box (5′-AAAAGNNNNNNNN-GAAAA-3′) present in the *ftsQ* promoter (Yamamoto *et al.*, 2001) and the *uvrY* promoter (Suzuki *et al.*, 2002), but detailed analysis of the protein–DNA interaction is beyond the scope of this study owing to the resolution of the SdiA–DNA complex model.

The most interesting observation in the dimeric model of *E. coli* SdiA is the position of Cys232 on helix α9, which possibly participates in the formation of an intermolecular disulfide bond with the same residue in the other subunit, since the distance between the two S atoms is 3.8 Å (Fig. 6*a*). This feature seems to be unique to SdiA since the multiple sequence alignment shows that only SdiA possesses Cys at this position (Fig. 1). Considering the relative distance and orientation of the two Cys232 residues in the SdiA dimer, it is assumed that an intermolecular disulfide bond is formed under oxidative conditions. As expected, disulfide-bond formation was

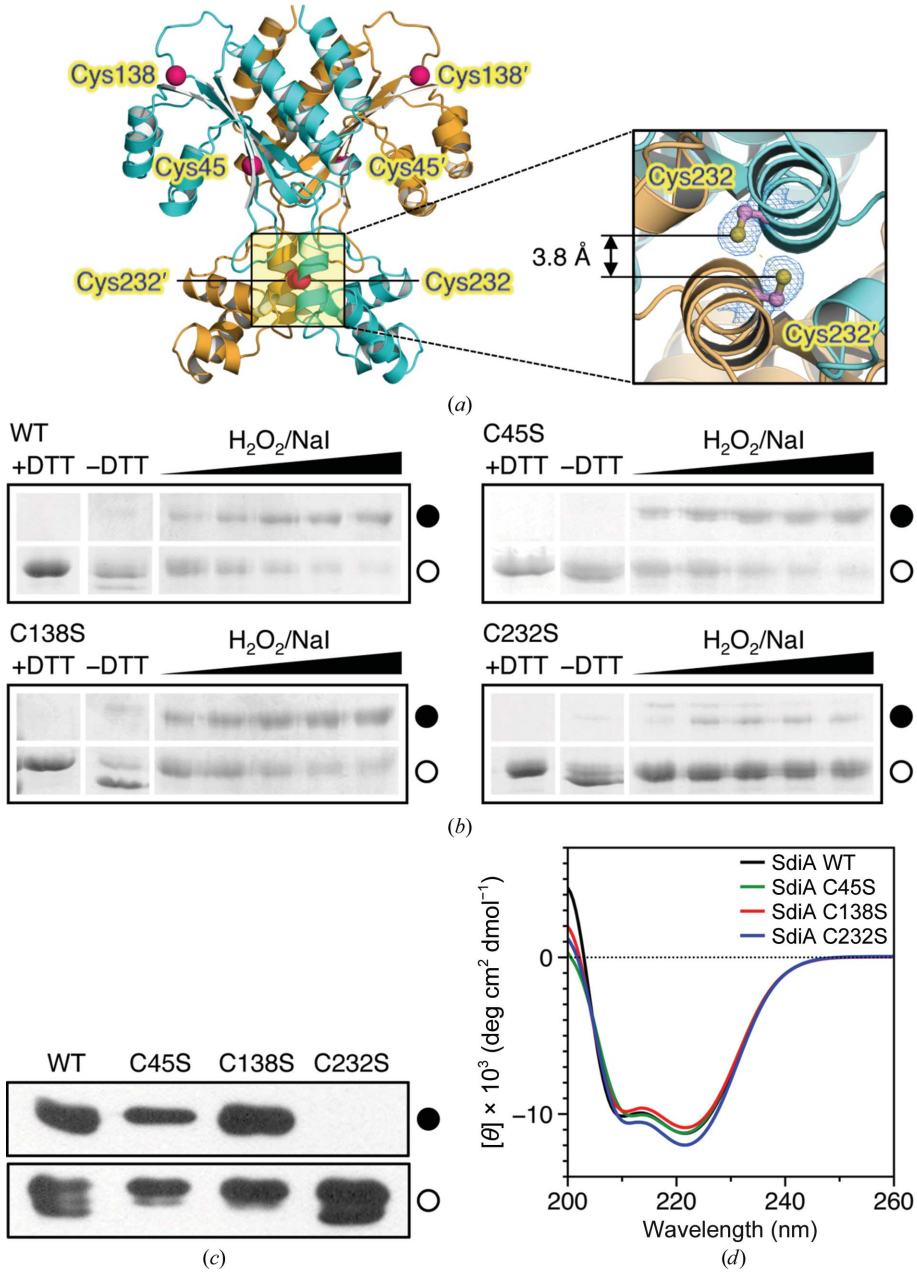

Figure 6
The involvement of Cys232 in the formation of a disulfide bond. (*a*) Positions of Cys residues are depicted in the dimeric structure of SdiA. The monomer subunits are drawn as cyan and orange ribbon diagrams, and the C^{α} atoms of Cys residues are illustrated as pink spheres. Inset, Cys232 residues are depicted by stick models along the axis parallel to the α9 helices. The electron-density maps of the Cys232 residues are contoured at the 1.0σ level and the distance between two S atoms is indicated. (*b*) Coomassie Blue-stained nonreducing SDS–PAGE of wild-type and Cys-mutant SdiA under oxidative conditions. H_2O_2/NaI in an equal molar ratio was used as an oxidizing agent and was added to reactions at final concentrations of 5, 10, 25, 50 and 100 m*M*. (*c*) Western blot analysis of wild-type and Cys-mutant SdiA using anti-His_6 antibody. The samples were electrophoresed under nonreducing conditions before transfer to a nitrocellulose membrane. In (*b*) and (*c*), closed and open circles indicate the positions of the dimer and monomer bands, respectively. (*d*) Circular-dichroism (CD) spectra of the wild-type and Cys-mutant SdiA. Each spectrum is a representative average of triplicate measurements.

enhanced by H_2O_2/NaI but was abolished by DTT (Fig. 6*b*), proving that the intermolecular disulfide bond was formed under oxidative conditions. Further supporting this finding, three Cys residues were individually mutated to Ser and oxidation-dependent dimer formation was examined. Consistently, among the three mutants, only the Cys232 mutant was insensitive to the oxidation environment (Fig. 6*b*). The activity change observed in the mutant protein is not caused by structural alteration but by the mutation at Cys232, because there was no significant conformational difference between the wild-type and the mutated proteins as determined by CD spectroscopy (Fig. 6*d*). To further confirm the disulfide-enhanced dimerization under conditions similar to the cellular environment, *E. coli* cell lysates containing each Cys mutant with a His_6 tag were immediately subjected to nonreducing SDS–PAGE and were analyzed by Western blotting with anti-His_6 antibody. Consistent with the results of the *in vitro* assay using the purified protein, the Cys232 mutant did not form a disulfide bond, while the other mutants formed dimers in cell lysates (Fig. 6*c*), supporting Cys232 as the key residue involved in intermolecular disulfide-bond formation in *in vitro* and *in vivo* conditions.

3.6. Binding affinity of SdiA to the promoters

To investigate the contribution of AHLs to the promoter-binding affinity of SdiA, the DNA-binding affinity of apo SdiA for the *ftsQ*P2 promoter was compared with those in the presence of C_4-HSL, C_8-HSL or C_{12}-HSL using a DNA gel-shift assay. To prevent the nonspecific DNA binding of SidA, poly(G–C) was introduced as a nonspecific competitor in the reaction. The AHL-bound SdiA showed the same gel-shift pattern as apo SdiA, suggesting that apo and AHL-bound SdiA have a similar binding affinity for DNA (Fig. 7*a*). Furthermore, the mobility of the *ftsQ*P2 promoter was insensitive to the acyl-chain lengths of the AHLs (Fig. 7*a*). These results suggest that AHL does not affect the binding activity of SdiA towards the DNA promoter.

In addition to the *ftsQAZ* operon, it has been reported that the *uvrY* gene, which is involved in the defence against reactive oxygen species (ROS), is also controlled by SdiA (Wei *et al.*, 2001; Van Houdt *et al.*, 2006). By observing the mobility shift of DNA in a concentration-dependent manner, we also confirmed the binding of SdiA to the *uvrY* promoter (Fig. 7*b*). Considering the role of UvrY in the defence mechanism against ROS, it is tempting to assume that UvrY expression is controlled by SdiA in an oxidation-dependent manner. To test this hypothesis, the DNA-binding affinity of SdiA for the *uvrY* promoter was examined in the presence of oxidizing or reducing agents. Full DNA migration was observed when the DNA promoter was treated with 0.25 µ*M* SdiA, and the same activity was observed when the samples were treated with 5 m*M* DTT (Fig. 7*b*). In contrast, the binding affinity of SdiA for the *uvrY* promoter was reduced when 2 m*M* H_2O_2 was introduced into the same assay (Fig. 7*b*). According to the dimeric model of SdiA based on the crystal structure and the mutant analyses, we confirmed that Cys232 plays an important role in disulfide-bond formation under oxidative conditions (Fig. 6). Taking the above findings together, it is assumed that intersubunit disulfide-bond formation through Cys232 under oxidative conditions might hinder the binding of SdiA to

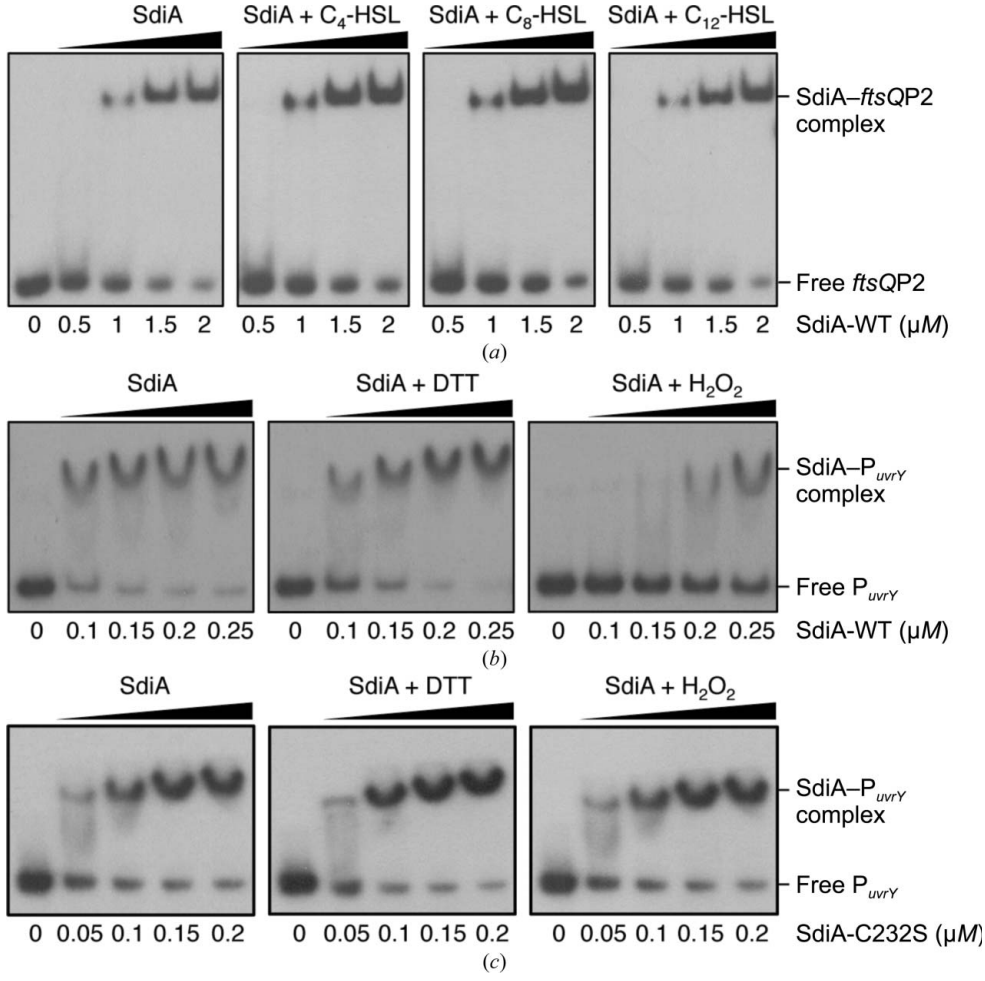

Figure 7
EMSA of SdiA on its target promoters. (*a*) Effect of AHLs on the binding affinity of SdiA to 54 bp *ftsQ*P2 promoter DNA. Reactions were carried out using 10 µ*M* C_4-HSL, C_8-HSL or C_{12}-HSL. (*b*) Binding of SdiA to 339 bp *uvrY* promoter DNA in the presence of reducing or oxidizing agents. (*c*) Binding of SdiA C232S mutant to the *uvrY* promoter DNA under reducing or oxidizing conditions. DTT (5 m*M*) and H_2O_2 (2 m*M*) were used as a reducing and an oxidizing agent, respectively.

Table 2
Disulfide-bond formation in bacterial oxidation-sensing transcription factors.

Protein	Bacterium	Residues	$C^{\beta}-C^{\beta}$ (Å)	References
SdiA	*Escherichia coli*	Cys232/Cys232′	5.7	This study
OxyR	*Escherichia coli*	Cys199/Cys208	17.0	Choi *et al.* (2001)
OhrR	*Xanthomonas campestris*	Cys22/Cys127′	13.5	Newberry *et al.* (2007)
CprK	*Desulfitobacterium dehalogenans*	Cys11/Cys200′ Cys105/Cys111	42.4 9.5	Joyce *et al.* (2006), Levy *et al.* (2008)
MosR	*Mycobacterium tuberculosis*	Cys10/Cys12	5.0	Brugarolas *et al.* (2012)
AgrA	*Staphylococcus aureus*	Cys199/Cys228	7.4	Sidote *et al.* (2008), Sun *et al.* (2012)

DNA. Consistently, the DNA-binding affinity of the Cys232 mutant for the *uvrY* promoter was not affected by either 5 m*M* DTT or 2 m*M* H_2O_2 (Fig. 7*c*). These results suggest that the transcriptional activity of SdiA towards the *uvrY* promoter is possibly controlled by the oxidation/reduction environment *via* Cys232. To further confirm the role of Cys232 in DNA binding, the effect of modification of Cys232 by the cysteine blocker methyl methanethiosulfonate (MMTS) was examined in the same gel-shift assay (Supplementary Fig. S5). MMTS treatment introduces a thiomethyl group into Cys232, which possibly perturbs the local conformational change near Cys232 and the packing of helix α9 between two subunits in dimeric SdiA. As expected, the DNA-binding activity of SdiA decreased in a concentration-dependent manner, suggesting that modified SdiA loses its DNA-binding activity.

4. Discussion

E. coli SdiA is known to respond to indole (Lee *et al.*, 2007) and to various AHL molecules released from other species (Ahmer, 2004). In this aspect, its ligand-binding specificity is relatively broad compared with those of other known LuxR-type receptors. In the current study, the structural basis for the broad substrate specificity of SdiA is provided: the ligand-binding site of SdiA is wide and open to the solvent and therefore SdiA can easily accommodate a wide range of ligands, even the low-molecular-weight PEG molecule. Although the substrate selectivity of SdiA is relatively broad, several findings indicate that *E. coli* SdiA has some selectivity for autoinducers. A biofilm-formation assay showed that *E. coli* SdiA responded to C_4-HSL, C_6-HSL and C_8-HSL but not to 3-oxo-C_8-HSL, C_{10}-HSL or C_{12}-HSL (Lee *et al.*, 2007). It has also been shown that AHLs with acyl groups containing six to eight C atoms are the most effective autoinducers for *Salmonella* SdiA (Michael *et al.*, 2001; Janssens *et al.*, 2007). The biochemical data presented here consistently revealed the selectivity of SdiA for ligands with short chain length (Fig. 5). In addition, the structure-based docking study of C_8-HSL and C_{10}-HSL to the ligand-binding site of SdiA provided a molecular basis for the binding selectivity of SdiA: Phe59 and Gln72 might act as occlusive residues of the ligand-binding cavity to limit the chain length of the acyl moiety to a maximum of eight C atoms (Fig. 5*b*). The binding mode of TEGs to the ligand-binding pocket of SdiA reveals that hydrophobic interactions are the determinants of their interaction, and thus ligands with longer acyl chains are likely to exhibit a higher binding affinity if they are accommodated. Isothermal titration calorimetric and thermal stability analyses strengthened our hypothesis by proving that the interaction of SdiA with C_8-HSL is stronger than that with C_4-HSL. Consistently, in the solution structure of the SdiA LBD with C_8-HSL, the acyl chain of C_8-HSL is well defined despite the conformational heterogeneity of the lactone moiety (Yao *et al.*, 2006). Since C_{10}-HSL exhibited a stabilizing effect on SdiA (Fig. 5*c*), we cannot rule out its interaction with SdiA. However, its effect is weaker than that of C_8-HSL because the T_m of SdiA-C_{10}-HSL is much lower than that of SdiA-C_8-HSL. In this case, the acyl tail of the AHL might induce a conformational change in occlusive residues such as Phe59 and Gln72 to prevent steric hindrance, which might in turn affect the conformation of the cavity and the binding affinity for the AHL.

AHLs are known to play a key role in the activation of QS receptors by stabilizing the overall folds of the receptors (Miller & Bassler, 2001), but it is not clear whether the AHL directly contributes to the binding affinity of the receptor for DNA. Moreover, the DNA-binding affinity of the apo and AHL-bound receptors has never been compared owing to the instability of the apo receptors. In this study, we were able to prepare intact homogenous apo SdiA and we demonstrated that AHLs do not affect the DNA-binding affinity of SdiA (Fig. 7*a*). These results are partially consistent with the high structural homogeneity of SdiA in the glycerol-bound and TEG-bound complexes, and suggest that the binding of AHLs to the SdiA LBD does not affect the conformation or function of the DBD (Fig. 7*a*). Therefore, it can be proposed that AHLs may play a role in controlling the transcriptional activity of SdiA by increasing their stability rather than by directly affecting their DNA-binding affinity. In this study, AHL-induced protein stabilization was also experimentally demonstrated for the first time by the increased melting temperature (T_m) of SdiA in the presence of AHLs (Fig. 5*c*).

Comparing the crystal structure of the intact *E. coli* SdiA with those of other AHL receptors revealed that the overall folds of the LBD and DBD of SdiA are well conserved with those in other LuxR-type QS receptors, whereas the relative orientations of the two domains are different. This observation strengthens the hypothesis of evolutionary combination of the two ancestral domains proposed in a previous study (Vannini *et al.*, 2002). At this time, it is not clear why the relative orientations of each domain are different in the LuxR-type receptors (Fig. 3*c*). However, considering the role of the AHL in stabilizing the LBD instead of conducting signals to the DBD, the conformational difference between TraR and SdiA (Fig. 3*b*) is not likely to be a result of ligand-induced conformational changes relevant to the transcriptional activity. Since the two SdiA structures obtained in different space groups (*C*2 and $P6_522$) are almost identical, we can also rule out the intrinsic conformational flexibility of the two

domains. Therefore, it is assumed that the relative orientation of each domain can be uniquely defined in each receptor. In support of this, the residues located in the interdomain interface are not conserved among AHL receptors (Fig. 1). Further biochemical and genetic studies need to be performed to elucidate the biological implications of the conformational diversity among AHL receptors.

Thiol-based redox sensing is one of the common mechanisms utilized by many bacterial transcription factors in response to oxidative stress in the surrounding environment (Antelmann & Helmann, 2011). In these cases, an interdisulfide or intradisulfide bond formed by the oxidation of reactive cysteine residues directly alters the structure and function of the corresponding transcription factors (Table 2). In the current study, a cysteine pair whose C^{β} atoms are 5.7 Å apart was observed in both the *C*2 and $P6_522$ crystal structures of *E. coli* SdiA. Compared with known oxidation-sensitive transcription factors, the inter-cysteine distance of SdiA is within the range of disulfide-bond formation (Table 2). Combining our structural and biochemical evidence with the role of UvrY in the ROS response (Wei *et al.*, 2001; Yamamoto *et al.*, 2001; Suzuki *et al.*, 2002; Van Houdt *et al.*, 2006), it is tempting to propose that the binding of SdiA to the *uvrY* promoter and the transcriptional activity of SdiA are controlled by the oxidative conditions, although we cannot rule out the possibility that disulfide-bond formation might be enforced in *in vitro* conditions. Further *in vivo* analyses are required to clarify the effect of the redox states of the cell, as well as the correlation between the AHL and redox signals to the activity of the QS receptor SdiA. Interestingly, the recent finding of the intramolecular disulfide redox switch in the quorum-sensing *agr* system supported the suggestion of the presence of cross-talk between QS and ROS signalling (Sun *et al.*, 2012).

In the current structural analyses of intact *E. coli* SdiA, we provide structural evidence for understanding not only the broad ligand selectivity of SdiA but also the general role of AHLs in QS receptors. Our study also proposes the possibility of the oxidation-dependent regulation of SdiA *via* Cys232. Moreover, as provided in this study, the crystal structures of SdiA in complex with a stabilizer provide a valuable template not only for the study of ligand identification by SdiA but also for the design of appropriate inhibitors.

This work was supported by National Research Foundation of Korea grants to KKK (2011-0028878) and HYH (2012R1A1A3010753).

References

Ahmer, B. M. (2004). *Mol. Microbiol.* **52**, 933–945.

Ahmer, B. M., van Reeuwijk, J., Timmers, C. D., Valentine, P. J. & Heffron, F. (1998). *J. Bacteriol.* **180**, 1185–1193.

Antelmann, H. & Helmann, J. D. (2011). *Antioxid. Redox Signal.* **14**, 1049–1063.

Bottomley, M. J., Muraglia, E., Bazzo, R. & Carfì, A. (2007). *J. Biol. Chem.* **282**, 13592–13600.

Brugarolas, P., Movahedzadeh, F., Wang, Y., Zhang, N., Bartek, I. L., Gao, Y. N., Voskuil, M. I., Franzblau, S. G. & He, C. (2012). *J. Biol. Chem.* **287**, 37703–37712.

Brünger, A. T., Adams, P. D., Clore, G. M., DeLano, W. L., Gros, P., Grosse-Kunstleve, R. W., Jiang, J.-S., Kuszewski, J., Nilges, M., Pannu, N. S., Read, R. J., Rice, L. M., Simonson, T. & Warren, G. L. (1998). *Acta Cryst.* D**54**, 905–921.

Chai, Y. & Winans, S. C. (2005). *J. Bacteriol.* **187**, 1219–1226.

Chen, G., Swem, L. R., Swem, D. L., Stauff, D. L., O'Loughlin, C. T., Jeffrey, P. D., Bassler, B. L. & Hughson, F. M. (2011). *Mol. Cell*, **42**, 199–209.

Choi, H., Kim, S., Mukhopadhyay, P., Cho, S., Woo, J., Storz, G. & Ryu, S. E. (2001). *Cell*, **105**, 103–113.

Fuqua, C., Winans, S. C. & Greenberg, E. P. (1996). *Annu. Rev. Microbiol.* **50**, 727–751.

Galloway, W. R., Hodgkinson, J. T., Bowden, S. D., Welch, M. & Spring, D. R. (2011). *Chem. Rev.* **111**, 28–67.

Galloway, W. R., Hodgkinson, J. T., Bowden, S., Welch, M. & Spring, D. R. (2012). *Trends Microbiol.* **20**, 449–458.

Greenfield, N. J. (2007). *Nature Protoc.* **1**, 2527–2535.

Hughes, D. T., Terekhova, D. A., Liou, L., Hovde, C. J., Sahl, J. W., Patankar, A. V., Gonzalez, J. E., Edrington, T. S., Rasko, D. A. & Sperandio, V. (2010). *Proc. Natl Acad. Sci. USA*, **107**, 9831–9836.

Humphrey, W., Dalke, A. & Schulten, K. (1996). *J. Mol. Graph.* **14**, 33–38.

Janssens, J. C., Metzger, K., Daniels, R., Ptacek, D., Verhoeven, T., Habel, L. W., Vanderleyden, J., De Vos, D. E. & De Keersmaecker, S. C. (2007). *Appl. Environ. Microbiol.* **73**, 535–544.

Jones, T. A., Zou, J.-Y., Cowan, S. W. & Kjeldgaard, M. (1991). *Acta Cryst.* A**47**, 110–119.

Joyce, M. G., Levy, C., Gábor, K., Pop, S. M., Biehl, B. D., Doukov, T. I., Ryter, J. M., Mazon, H., Smidt, H., van den Heuvel, R. H., Ragsdale, S. W., van der Oost, J. & Leys, D. (2006). *J. Biol. Chem.* **281**, 28318–28325.

Kanamaru, K., Kanamaru, K., Tatsuno, I., Tobe, T. & Sasakawa, C. (2000). *Mol. Microbiol.* **38**, 805–816.

Laskowski, R. A., MacArthur, M. W., Moss, D. S. & Thornton, J. M. (1993). *J. Appl. Cryst.* **26**, 283–291.

Lee, J., Jayaraman, A. & Wood, T. K. (2007). *BMC Microbiol.* **7**, 42.

Levy, C., Pike, K., Heyes, D. J., Joyce, M. G., Gabor, K., Smidt, H., van der Oost, J. & Leys, D. (2008). *Mol. Microbiol.* **70**, 151–167.

Lintz, M. J., Oinuma, K., Wysoczynski, C. L., Greenberg, E. P. & Churchill, M. E. (2011). *Proc. Natl Acad. Sci. USA*, **108**, 15763–15768.

Marketon, M. M., Gronquist, M. R., Eberhard, A. & González, J. E. (2002). *J. Bacteriol.* **184**, 5686–5695.

Michael, B., Smith, J. N., Swift, S., Heffron, F. & Ahmer, B. M. (2001). *J. Bacteriol.* **183**, 5733–5742.

Miller, M. B. & Bassler, B. L. (2001). *Annu. Rev. Microbiol.* **55**, 165–199.

Murshudov, G. N., Skubák, P., Lebedev, A. A., Pannu, N. S., Steiner, R. A., Nicholls, R. A., Winn, M. D., Long, F. & Vagin, A. A. (2011). *Acta Cryst.* D**67**, 355–367.

Nasser, W. & Reverchon, S. (2007). *Anal. Bioanal. Chem.* **387**, 381–390.

Nealson, K. H. & Hastings, J. W. (1979). *Microbiol. Rev.* **43**, 496–518.

Newberry, K. J., Fuangthong, M., Panmanee, W., Mongkolsuk, S. & Brennan, R. G. (2007). *Mol. Cell*, **28**, 652–664.

Otwinowski, Z. & Minor, W. (1997). *Methods Enzymol.* **276**, 307–326.

Rahmati, S., Yang, S., Davidson, A. L. & Zechiedrich, E. L. (2002). *Mol. Microbiol.* **43**, 677–685.

Rasmussen, T. B. & Givskov, M. (2006). *Int. J. Med. Microbiol.* **296**, 149–161.

Ravichandiran, V., Shanmugam, K., Anupama, K., Thomas, S. & Princy, A. (2012). *Eur. J. Med. Chem.* **48**, 200–205.

Sabag-Daigle, A., Soares, J. A., Smith, J. N., Elmasry, M. E. & Ahmer, B. M. (2012). *Appl. Environ. Microbiol.* **78**, 5424–5431.

Sidote, D. J., Barbieri, C. M., Wu, T. & Stock, A. M. (2008). *Structure*, **16**, 727–735.
Sitnikov, D. M., Schineller, J. B. & Baldwin, T. O. (1996). *Proc. Natl Acad. Sci. USA*, **93**, 336–341.
Skilbeck, C. A., Pumbwe, L. & Wexler, H. M. (2009). *Current Trends in Antibiotic Resistance in Infectious Diseases*, edited by A. U. Khan, pp. 1–24. New Delhi: I. K. International Publishing House.
Smith, J. N., Dyszel, J. L., Soares, J. A., Ellermeier, C. D., Altier, C., Lawhon, S. D., Adams, L. G., Konjufca, V., Curtiss, R. III, Slauch, J. M. & Ahmer, B. M. (2008). *PLoS One*, **3**, e2826.
Sperandio, V. (2010). *Gut Microbes*, **1**, 432–435.
Sun, F., Liang, H., Kong, X., Xie, S., Cho, H., Deng, X., Ji, Q., Zhang, H., Alvarez, S., Hicks, L. M., Bae, T., Luo, C., Jiang, H. & He, C. (2012). *Proc. Natl Acad. Sci. USA*, **109**, 9095–9100.
Suzuki, K., Wang, X., Weilbacher, T., Pernestig, A. K., Melefors, O., Georgellis, D., Babitzke, P. & Romeo, T. (2002). *J. Bacteriol.* **184**, 5130–5140.
Terwilliger, T. C. (2000). *Acta Cryst.* D**56**, 965–972.
Terwilliger, T. C. (2003). *Acta Cryst.* D**59**, 38–44.
Terwilliger, T. C. & Berendzen, J. (1999). *Acta Cryst.* D**55**, 849–861.
Vagin, A. & Teplyakov, A. (2010). *Acta Cryst.* D**66**, 22–25.
Van Houdt, R., Aertsen, A., Moons, P., Vanoirbeek, K. & Michiels, C. W. (2006). *FEMS Microbiol. Lett.* **256**, 83–89.
Vannini, A., Volpari, C., Gargioli, C., Muraglia, E., Cortese, R., De Francesco, R., Neddermann, P. & Marco, S. D. (2002). *EMBO J.* **21**, 4393–4401.
Wang, X. D., de Boer, P. A. & Rothfield, L. I. (1991). *EMBO J.* **10**, 3363–3372.
Wei, Y., Lee, J. M., Smulski, D. R. & LaRossa, R. A. (2001). *J. Bacteriol.* **183**, 2265–2272.
Whitehead, N. A., Barnard, A. M., Slater, H., Simpson, N. J. & Salmond, G. P. (2001). *FEMS Microbiol. Rev.* **25**, 365–404.
Wu, C., Lokanath, N. K., Kim, D. Y., Nguyen, L. D. N. & Kim, K. K. (2008). *Acta Cryst.* F**64**, 19–21.
Yamamoto, K., Yata, K., Fujita, N. & Ishihama, A. (2001). *Mol. Microbiol.* **41**, 1187–1198.
Yao, Y., Martinez-Yamout, M. A., Dickerson, T. J., Brogan, A. P., Wright, P. E. & Dyson, H. J. (2006). *J. Mol. Biol.* **355**, 262–273.
Zhang, R.-G., Pappas, K. M., Pappas, T., Brace, J. L., Miller, P. C., Oulmassov, T., Molyneaux, J. M., Anderson, J. C., Bashkin, J. K., Winans, S. C. & Joachimiak, A. (2002). *Nature (London)*, **417**, 971–974.
Zhu, J. & Winans, S. C. (1999). *Proc. Natl Acad. Sci. USA*, **96**, 4832–4837.
Zhu, J. & Winans, S. C. (2001). *Proc. Natl Acad. Sci. USA*, **98**, 1507–1512.